Broadside-Coupled Filtering Circular Patch Power Dividers

Y-Chun Khor, Eng-Hock Lim[*], Boon-Kuan Chung

Abstract—Broadside coupling mechanism between different patch resonators is deployed for designing power dividers to provide bandpassing effect. To demonstrate, two sector-shaped patches are combined and concentrically stacked on top of a circular microstrip resonator where pairs of concentric arc-shaped slots and radial notches are etched to perturb the current distribution so that an additional pole can be obtained to broaden the operational bandwidth. The use of circular patch enables the expansion of output ports without increasing the design complexity. Also, it was found that broadside coupling generates transmission zeros which can be used to sharpen the rolloff skirt for a better selectivity. In this paper, the corresponding design theory and methodology are elucidated, together with the detailed parametric analysis.

1. INTRODUCTION

Circular patch resonator was first proposed by Watkins [1] in 1969. Because of its simplicity, it has been used for designing many types of microwave components. In the early 70s, however, the microstrip patch was more commonly deployed as a lumped capacitor because of its stable response, due to excellent field confinement between the metal patches at low frequencies [2, 3]. It was Long et al. who first explored the radiation modes of the circular patch for a multitude of antennas [4], with the cavity model and field analysis available in [5]. Since the mid-80s, the non-radiating resonances of the circular patch have gained much attention because of its ability to provide broad microwave bandwidth. In [6], multiple feedlines were connected to the patch to make it a multi-functional and multi-port power divider and crossover. To estimate its resonant frequency more accurately, the effect of fringing field around the patch perimeter was later accounted for in [7, 8]. Being planar in structure and easy to integrate with other active devices, the circular patch was made a radial combiner/divider [9] to incorporate with power amplifiers for boosting up microwave power in the late 80s.

It is obvious that the circular microstrip patch resonator has been of great interest over the past four decades because of its advantages such as simplicity, compactness, versatility, as well as the ability to excite multiple resonances in a single piece. However, there is only one physical design parameter — radius to tune in this structure. This makes the optimization process very difficult. Although the patch can usually provide wide bandwidth, the frequency selectivity of some of the modes can be very poor due to low Q factor. Having sharp rolloff skirt around the cutoff frequencies is very desirable for improving the out-of-band rejection [10] of a wireless system. Conventionally, filtering effect can be imposed by cascading a bandpass filter to either the input or output feedline of a circuit [11–14], with the price of larger footprint and higher complexity. Effort was also made to embed a filtering structure into another component for shaping the rolloff near the passband edges, but it requires the use of an external lumped resistor [15]. Recently, the left- and right-handed elements were carefully combined to design a diplexer that has filtering response [16]. But the design is very complex.

In this paper, a circular microstrip patch resonator, coupled with two concentric top-loading sector-shaped patches, is deployed for designing a broadband and multiple-output power divider. Arc-shaped

slots and radial notches are introduced on the patch to excite the higher-order TM_{n10}^z, $n \geq 2$ for generating an additional pole, as well as for optimizing the resonant frequencies of zeros. It was found that broadside coupling fields between the patches generate two zeros that help improve frequency selectivity. Combining the circular and sector-shaped patches in such a way enables the power divider to have multiple outputs without increasing the design complexity. Also, it is much simpler as no isolation resistor is required. In this paper, all the structures were simulated using Ansoft HFSS software, whereas measurement was conducted using an R&S®ZVB8 Vector Network Analyzer (VNA). In experiments, the unused ports were always terminated by the 50-Ω loads.

2. CIRCUIT CONFIGURATION

Figure 1 illustrates the schematic of the proposed one-to-two power divider, which is made on a Duroid RO4003C substrate with thickness of $h = 1.524$ mm and dielectric constant of $\varepsilon_r = 3.38$. The bottom patch resonator (with radius of $R_a = 15$ mm), sandwiched in between *Substrate* 1 and 2, is etched with a pair of arc-shaped slots and two pairs of radial notches. Each of the slots has a length of $c = 8.2$ mm and a width of $d = 0.5$ mm. They are placed concentrically and opposite with $e = 9.5$ mm from the center of the patch. Two pairs of radial notches, which are cut symmetrically along the patch perimeter, have the dimensions of $a = 5$ mm, $\theta_a = 64.6°$, $b = 10.5$ mm, and $\theta_b = 38.6°$ as shown in Fig. 1(a). This resonator is excited by an input coaxial feed (Port 1) connected to the center of the patch. Fig. 1(b) depicts the top view of the sector-shaped patch which is made on *Substrate* 2 to couple the electromagnetic signal out to the two output ports (Port 2 and Port 3). It consists of two identical metallic sectors of $R_b = 15$ mm and $\theta_t = 90°$, both of which are functioning as an embedded quarter-wavelength impedance transformer. To further improve the impedance matching, a small circular patch ($R_c = 1$ mm) is centrally included to the top patch. Microwave signal from Port 1 can then be guided to the two 50-Ω microstrip lines
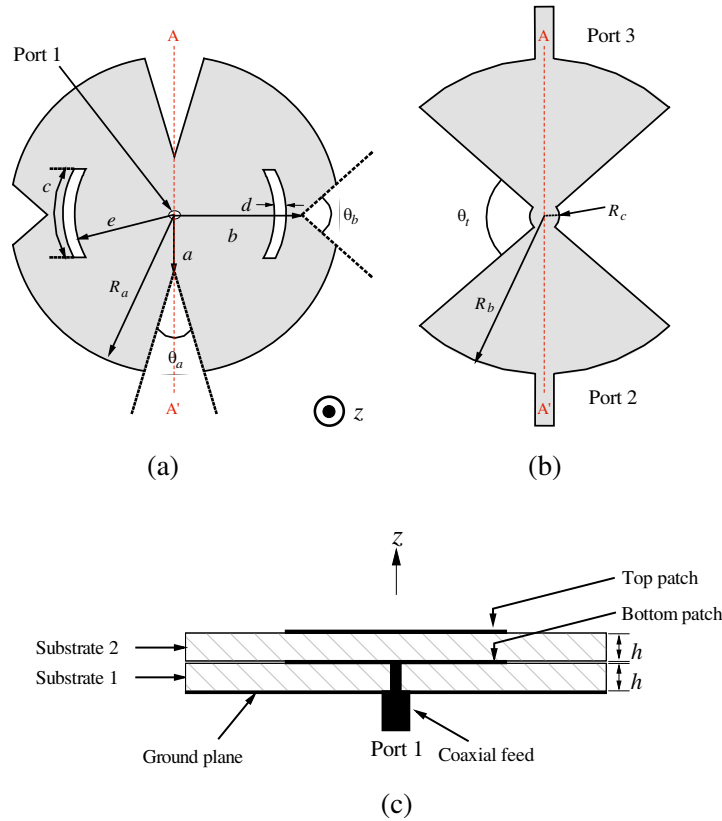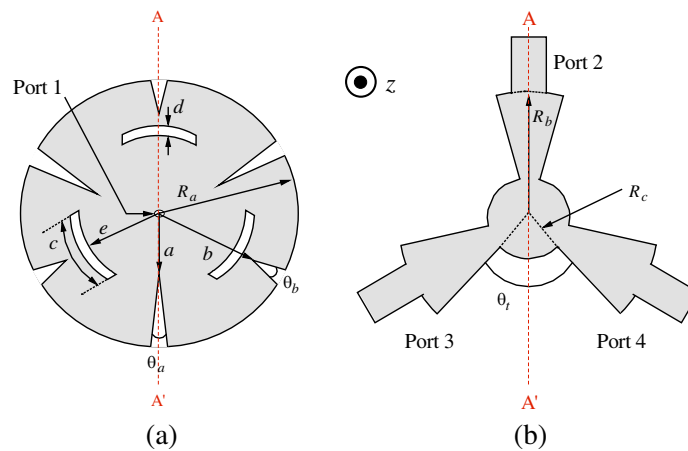

Figure 1. Schematic of the proposed one-to-two bandpassing power divider. (a) Bottom patch; (b) Top patch; (c) Side view.

at the output ports (Port 2 and 3). Both the patches share the common ground on the bottom-most surface and they must be properly aligned along line A-A' for maximum coupling. Fig. 2 shows the manufactured prototype.
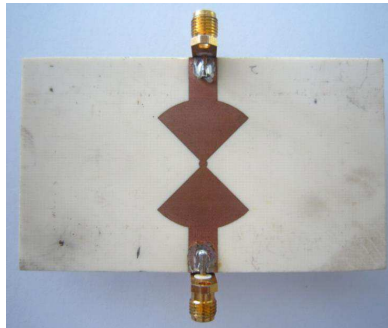
Figure 2. Photograph of the prototype of the proposed one-to-two bandpassing power divider.

The schematic of the proposed one-to-three power divider is illustrated in Fig. 3. Again, both the top and bottom patches ($R_a = R_b = 15$ mm) are sharing the same ground plane. The bottom patch placed on *Substrate* 1 is excited by a coaxial-feed port (Port 1). For this configuration, it has three arc slots ($d = 0.5$ mm, $c = 6.2$ mm) along with two sets of sector-shaped notches (θ_a and θ_b), which are $120°$ apart from each other. The slots are centered at the origin (with $e = 9.5$ mm) of the resonator. The dimension of the notches is given by $\theta_a = 8.2°$, $\theta_b = 14.3°$, $a = 8$ mm and $b = 11$ mm. With reference to Fig. 3(b), three sector-shaped metallic patches ($R_b = 15$ mm and $\theta_t = 93.7°$), made on *substrate* 2, are used to couple microwave signals to the output ports. Again, a small circular patch with radius of $R_c = 5$ mm is placed at the center of the output patch for improving the impedance matching as well as for optimizing the transmission zero position. Again, the two patches are aligned along the line A-A'.

(a) (b)

Figure 3. Schematic of the proposed one-to-three bandpassing power divider. (a) Bottom patch; (b) Top patch.

3. DESIGN AND ANALYSIS

It is very important to understand the properties of a circular patch resonator since the bottom patch is made out of it. A simple circular microstrip resonator, with radius of $R_a = 15$ mm (substrate thickness of $h = 1.524$ mm and dielectric constant of $\varepsilon_r = 3.38$) centrally fed by a single coaxial probe, is studied first. It was observed from simulation that this simple patch only has a transverse TM_{010}^z mode resonating at the frequency of 6.4 GHz below 8 GHz. By including a pair of arc-shaped narrow slots and two pairs radial notches (with the design parameters identical to the bottom patch of the one-to-two power

divider), this resonator can now generate two resonances, TM_{210}^z and TM_{010}^z, respectively at 5.56 and 6.22 GHz, as shown in Fig. 4. The surface current distributions on this simple patch are simulated in Fig. 5. It is very interesting to observe from Fig. 5(a) that the horizontal pairs of radial notches and arc slots enable the excitation of TM_{210}^z resonance. Also, the current distributions in Fig. 5(b) shows that the existence of the four radial notches does not jeopardize the TM_{010}^z mode. The resonant frequency for the TM_{mno}^z mode of a simple circular microstrip patch resonator can be calculated using (1) [17, 18].

$$f_{mn0} = \frac{\chi_{mn}c}{2\pi R_e \sqrt{\varepsilon_{reff}}} \tag{1}$$

$\chi_{mn} = k_{mn}R_a$ is the mth — order zero of $J_n'(kR_a)$, c the velocity of light in free space, and $\varepsilon_{reff} \approx (1+\varepsilon_r)/2$ the substrate's effective relative permittivity. The effective radius R_e has accounted for the virtual width caused by the fringing field around the perimeter of the circular patch and it can be calculated using the empirical formula [18] in (2). For a simple circular patch with $R_a = 15$ mm, $h = 1.524$ mm, and $\varepsilon_r = 2.33$, the resonant frequencies of the two modes are calculated to be $f_{210} = 5.11$ GHz and $f_{010} = 6.04$ GHz (with $\chi_{01} = 3.83171$ and $\chi_{21} = 3.05424$). The simulated resonant frequencies for the slotted and notched patch, as can be seen in Fig. 4, are slightly higher than those for the simple circular patch. The double-layered power divider (Fig. 1) can be easily constructed by top-loading the top patch, along with *Substrate* 2, onto the circular patch in Fig. 4.

$$R_e = R_a \sqrt{1 + \frac{2h}{\pi R_a}\left[\ln\left(\frac{\pi R_a}{2h}\right) + 1.7726\right]}, \quad m \neq 0 \tag{2a}$$
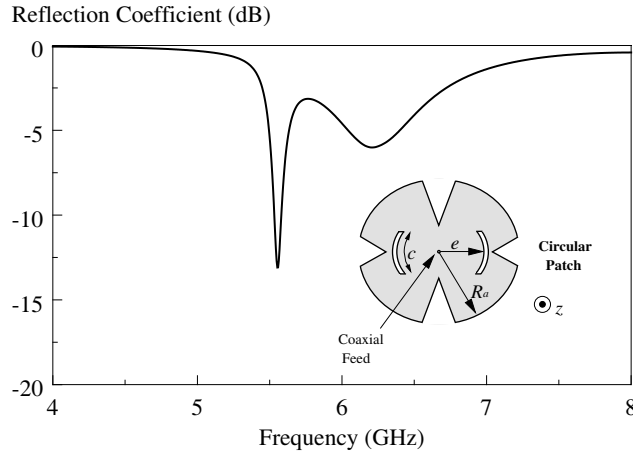
Figure 4. Circular patch with a pair of circumferential narrow slots and two pairs of radial notches.
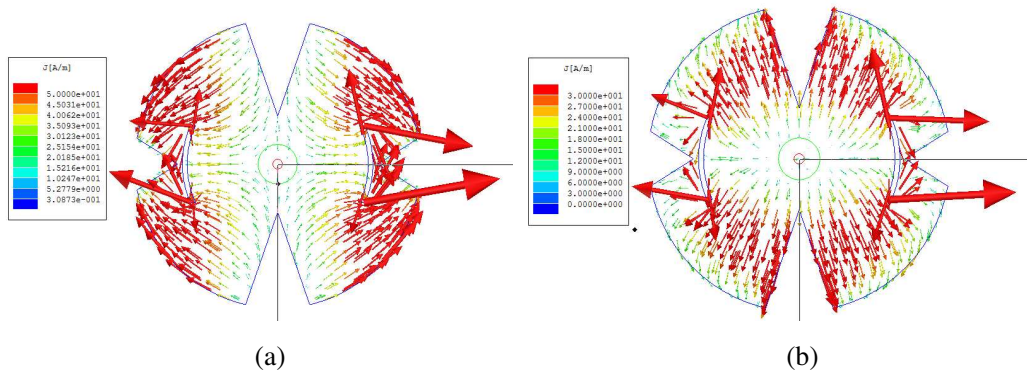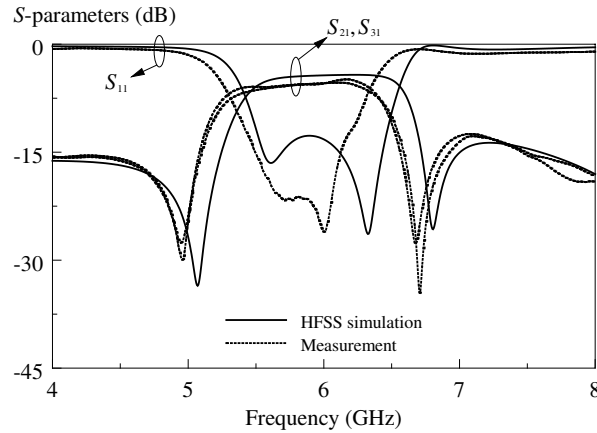

Figure 5. Surface current distributions of the (a) TM_{210}^z mode at 5.56 GHz, (b) TM_{010}^z mode at 6.22 GHz of the one-port simple circular microstrip resonator with slots and notches.

$$R_e = R_a \sqrt{1 + \frac{2h}{\pi \varepsilon_r} \left[\ln \left(\frac{R_a}{2h} + \frac{h}{R_a} \left(0.268 \varepsilon_r + 1.65 \right) + \sqrt{2} \varepsilon_r + 1.7726 \right) \right]}, \quad m = 0 \qquad (2b)$$

4. RESULTS AND DISCUSSION

Figure 6 depicts the simulated and measured reflection and transmission coefficients of the proposed one-to-two power divider (in Fig. 1). The measured center frequency reads 5.85 GHz (simulation 6.03 GHz), with two poles at $P_1 = 5.77$ GHz and $P_2 = 6$ GHz. In general, the measured result agrees reasonably well with simulation. The measured fractional bandwidth (FBW) is 12.49% (simulation 15.25%), with an insertion loss of ~ -5.5 dB at the center frequency. The resonances TM_{210}^z and TM_{010}^z are clearly seen inside the passband, as can be justified from the current distributions on the bottom patch at the two poles (in Fig. 7), which are very close to those in Fig. 5. The simulated insertion loss is slightly higher than its measured value as it does not account for the losses caused by the SMA connectors and patch conductors. It is interesting to note that two transmission zeros are available at $Z_1 = 4.95$ GHz (simulation 5.07 GHz) and $Z_2 = 6.7$ GHz (simulation 6.8 GHz) in measurement near both the cutoff frequencies, improving the selectivity performance significantly. They are caused by the tight coupling between the bottom and top patches. The electric field distributions of the zeros are illustrated in Fig. 8. Compared with the pole currents of P_1 and P_2, transmission zeroes Z_1 and Z_2 are the coupled modes of their corresponding nearby poles seen from the field patterns.


Figure 6. Measured, simulated reflection and transmission coefficients of the proposed one-to-two bandpassing power divider.
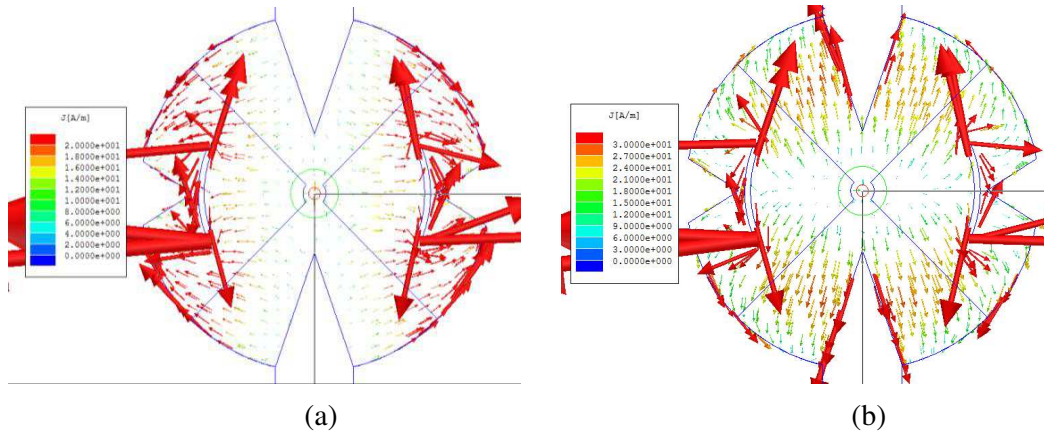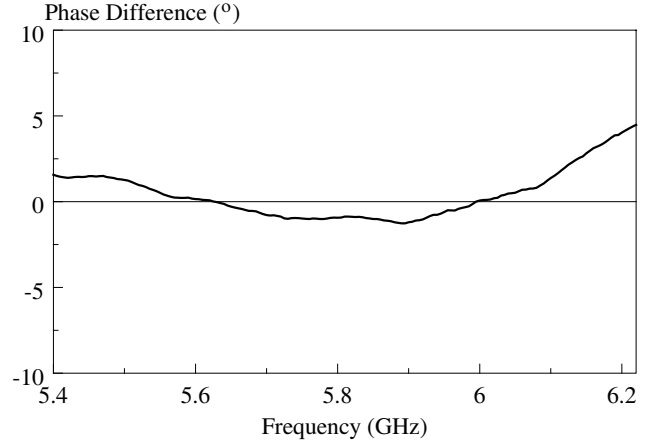

Figure 7. Simulated current distributions of the power divider on the bottom patch. (a) Pole P_1 (TM_{210}^z mode) at 5.62 GHz, (b) Pole P_2 (TM_{010}^z mode) at 6.32 GHz.
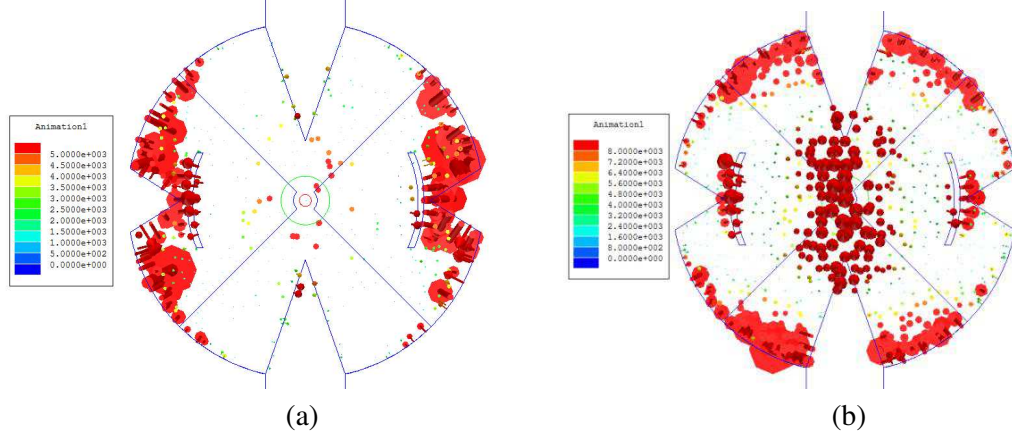
Figure 8. Simulated electric field distributions for the structure for (a) zero Z_1 at 5.07 GHz, (b) zero Z_2 at 6.8 GHz.
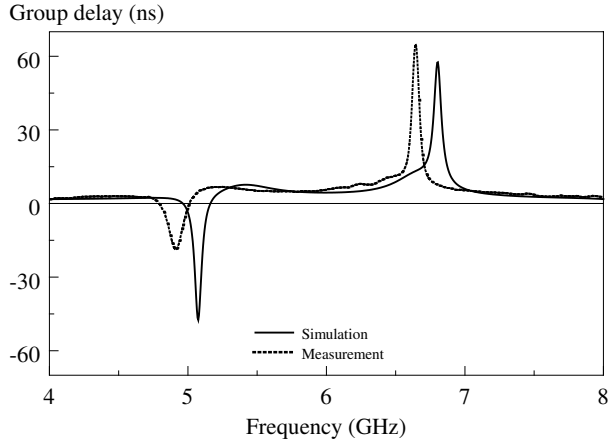
Figure 9. Simulated and measured group delays of the proposed one-to-two bandpassing power divider.

Figure 10. Phase difference between the two output signals of the proposed one-to-two bandpassing power divider.

     Figure 9 shows the simulated and measured group delays ($\tau_{d21} = \frac{d\phi_{21}}{df}$) of the proposed power divider, showing almost a constant delay inside the passband. Because of its symmetry, τ_{d31} is very close to τ_{d21}, and the result is omitted here. This is very positive as it implies the proposed power divider does not cause any distortion to the input signal even in such a broad bandwidth. The phase difference ($\angle S_{21} - \angle S_{31}$), calculated from the measured $\angle S_{21}$ and $\angle S_{31}$, between the two output signals is shown in Fig. 10, showing that they are in-phase with a difference of less than $5°$ across the entire passband.

     Parametric analysis has been performed to visualize the effects of the slots and notches on the poles and zeros. It is interesting to note that all the poles and zeros can be tuned and optimized almost independently. First, the radial length of the circumferential narrow slot is studied. As can be seen from Fig. 11, longer c can cause the resonant frequencies of the pole (P_1) and zero (Z_1) to reduce from 5.74 to 5.44 and 5.15 to 4.94 GHz, respectively. This is not surprising since the patch has high current and electric field densities around the positions of the two slots, as can be seen from Figs. 7(a) and 8(a). It is also a fact that the current path on the bottom patch becomes longer for a greater c value, resulting in a lower resonant frequency. The design parameter does not affect P_2 and Z_2 much.

     Figure 12 shows variation in frequency corresponding to the change in the radial notch angle θ_b. It is observed that P_1 and Z_1 resonances can be made lower by having a smaller angle. But it does not change P_2 and Z_2 much. This is very encouraging as it implies that the P_1 and Z_1 frequencies can
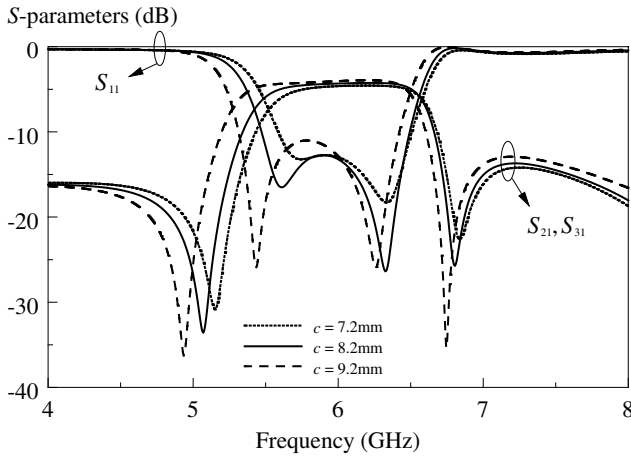
Figure 11. Effect of the arc-shaped slot length c on the frequency response of the one-to-two power divider.
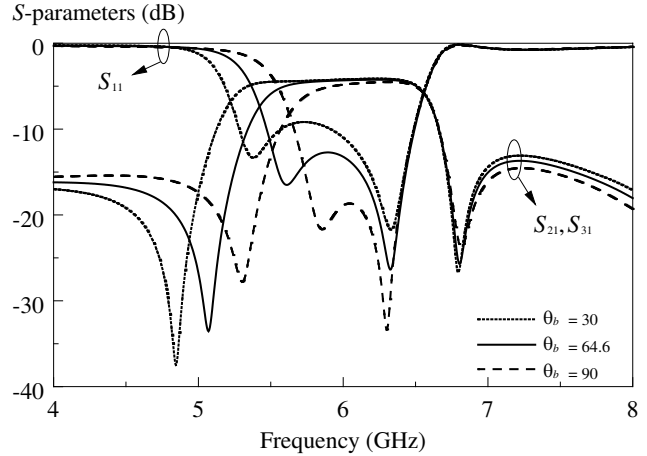
Figure 12. Effect of the radial notch angle θ_b on the frequency response of the one-to-two power divider.

Table 1. The perimeter of the bottom patch with respect to θ_b. The corresponding zero and pole frequencies are also appended.

| Angle of shallow notches, θ_b (deg)	Total perimeter of bottom patch (mm)	Z_1 (GHz)	P_1 (GHz)
30.0	135.00	4.85	5.38
64.6	130.68	5.08	5.61
90.0	127.74	5.31	5.86

Table 2. The perimeter of the bottom patch with respect to θ_a. The corresponding zero and pole frequencies are also appended.

| Angle of deep notches, θ_a (deg)	Total perimeter of bottom patch (mm)	Z_2 (GHz)	P_2 (GHz)
10	138.10	6.74	6.17
38.6	130.69	6.81	6.33
85	116.49	6.95	6.86

be tuned almost independently of P_2 and Z_2. Reducing this angle is actually causing the perimeter, shown in Table 1, of the patch to increase. Smaller θ_b corresponds to a longer current path along the perimeter, causing lower frequencies in both Z_1 and P_1. As can be seen in Figs. 7 and 8, again, the effect of θ_b is eminent as the current and fields are denser around both the shallow notches.

The effect of the notch angle θ_a is now studied. With reference to Fig. 13. It is noted that P_2 frequency increases with angle which corresponds to shorter perimeter. In general, Z_2 is also higher for shorter perimeter. Table 2 gives, at a glance, the relationship between θ_a and the frequencies of the upper pole and zero (Z_2 and P_2). Again, it does not affect P_1 and Z_1 much, justifiable from the high current and field concentration around the deep notches in Figs. 7 and 8. Another parameter found to affect upper zero is the radius R_c of the circular top patch. With reference to Fig. 14, it is observed that the Z_2 frequency reduces from 6.81 to 6.51 as R_c goes larger. It slightly affects the impedance matching of the P_2 resonance, but not the frequency.

As can be summarized, the lower pole P_1 and zero Z_1 near the lower cutoff frequency can be independently tuned by adjusting c and θ_b. On the other hand, the resonances of the upper pole P_2 and zero Z_2 can be optimized by tuning θ_a and R_c, without affecting the lower ones.
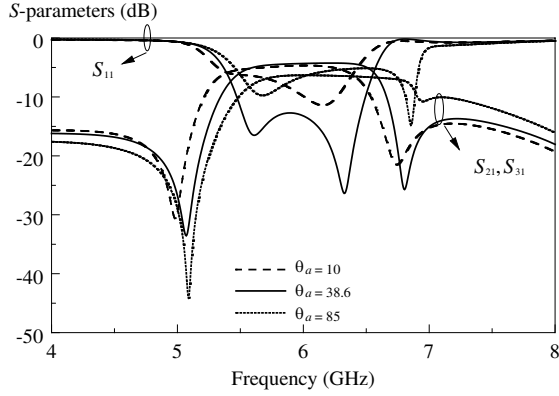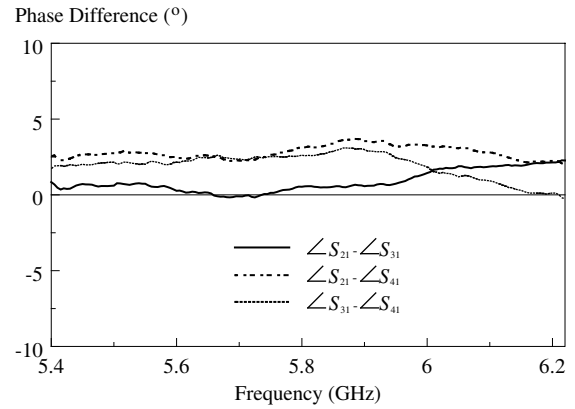
Figure 13. Effect of the radial notch angle θ_a on the frequency response of the one-to-two power divider.
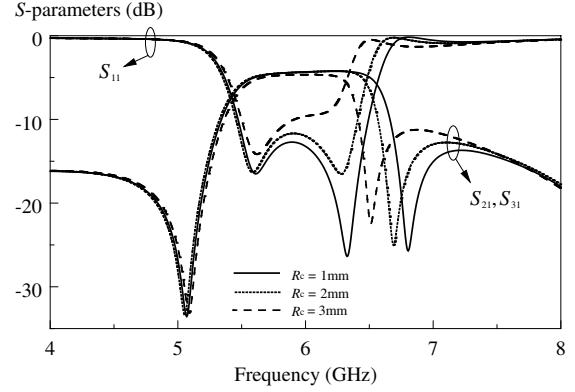
Figure 14. Effect of radius R_c on the frequency response of the one-to-two power divider.
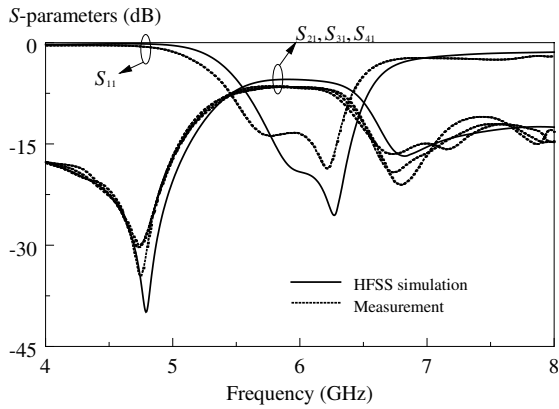
Figure 15. Measured, simulated reflection and transmission coefficients of the proposed one-to-three bandpassing power divider.

Figure 16. Phase differences between the three output ports of the proposed one-to-three bandpassing power divider.

Figure 15 shows the simulated and measured frequency responses of the proposed one-to-three power divider. Two poles in the passband are found to be the transverse TM^z_{010} and TM^z_{310} modes at 5.92 and 6.28 GHz, respectively. It was found from simulation that the three arc-shaped slots make the excitation of TM^z_{310} possible. Again, two transmission zeros are clearly seen near the cut-off frequencies (4.74 and 6.80 GHz). Measurement and simulation show that this power divider has a constant time delay across the entire passband. This is very interesting as it shows that the proposed design is very versatile! It can give good response, with double resonances with two zeros near the edges of the passband, even with multiple outputs as the excitation of the second pole (TM^z_{n10}, $n \neq 0$) is always possible. Again, the calculated phase differences ($\angle S_{21} - \angle S_{31}$), ($\angle S_{21} - \angle S_{41}$), and ($\angle S_{31} - \angle S_{41}$) between the three output signals are shown in Fig. 16, with an error less than $5°$ from 4 GHz to 8 GHz.

5. CONCLUSIONS

In this paper, two wideband multilayered bandpassing power dividers with high selectivity have been proposed. Arc-shaped slots and radial notches are introduced on the circular microstrip patch resonator to enable the excitation of the TM^z_{210} mode, broadening the fractional bandwidth. Broadside coupling mechanism enables the generation of two transmission zeroes near the cut-off frequencies which significantly improves the selectivity. Also, the proposed configuration is very compact as it does not require the use of any isolation resistors. In this paper, the reflection and transmission coefficients, along with other crucial design parameters, have been investigated.

ACKNOWLEDGMENT

REFERENCES

1. Watkins, J., "Circular resonant structures in microstrip," *Electron. Lett.*, Vol. 5, No. 21, 524–525, Oct. 1969.

2. Wolff, I. and N. Knoppik, "Rectangular and circular microstrip disk capacitors and resonators," *IEEE Trans. Microw. Theory Tech.*, Vol. 22, No. 10, 857–864, Oct. 1974.

3. Itoh, T. and R. Mittra, "A new method for calculating the capacitance of a circular disk for microwave integrated circuits," *IEEE Trans. Microw. Theory Tech.*, Vol. 22, No. 6, 431–432, Jun. 1973.

4. Long, S. A., L. C. Shen, and P. B. Morel, "Theory of the circular-disc printed-circuit antenna," *Proc. IEE*, Vol. 125, No. 10, 925–928, Oct. 1978.

5. Derneryd, A. G., "Analysis of the microstrip disk antenna element," *IEEE Trans. Antennas Prop.*, Vol. 27, No. 5, 660–664, Sep. 1979.

6. Gupta, K. C. and M. Abouzahra, "Analysis and design of four-port and five-port microstrip disc circuits, "*IEEE Trans. Microw. Theory Tech.*, Vol. 33, No. 12, 1422–1428, Dec. 1985.

7. Abouzahra, M. D. and K. C. Gupta, "Multiple-port power divider/combiner circuits using circular microstrip disk configurations," *IEEE Trans. Microw. Theory Tech.*, Vol. 35, No. 12, 1296–1302, Dec. 1987.

8. Bonetti, R. R. and P. Tiss, "Analysis of planar disk networks," *IEEE Trans. Microw. Theory Tech.*, Vol. 26, No. 7, 471–477, Jul. 1978.

9. Belohoubek, E., R. Brown, H. Johnson, A. Fathy, D. Bechtle, D. Kalokitis, and E. Mykietyn, "30-way radial power combiner for miniature GaAs FET power amplifiers," *IEEE MTT-S Int. Dig.*, 515–518, 1986.

10. Lin, F., Q. X. Chu, and S. W. Wong, "Design of dual-band filtering quadrature coupler using $\lambda/2$ and $\lambda/4$ resonators," *IEEE Microw. Wireless Comp. Lett.*, Vol. 22, No. 11, 565–567, Nov. 2012.

11. Llorente-Romano, S., A. Garcia-Lamperez, M. Salazar-Palma, A. I. Daganzo-Eusebiot, J. S. Galaz-Villasantet, and M. J. Padilla-Cruz, "Microstrip filter and power divider with improved out-of-band rejection for a Ku-band input multiplexer," *33rd European Microwave Conference*, 315–318, 2003.

12. Wong, S. W. and L. Zhu, "Ultra-wideband power dividers with good isolation and improved sharp roll-off skirt," *IET Microw. Antennas Propag.*, Vol. 3, No. 8, 1157–1163, 2008.

13. Arriola, W. A., J. Y. Lee, and I. S. Kim, "Wideband 3 dB branch line coupler based on open circuited coupled lines," *IEEE Microw. Wireless Comp. Lett.*, Vol. 21, No. 9, 486–488, Sep. 2011.

14. Deng, P. H. and L. C. Lai, "Unequal wilkinson power dividers with favorable selectivity and high-isolation using coupled-line filter transformers," *IEEE Trans. Microw. Theory Tech.*, Vol. 60, No. 6, 1520–1529, Jun. 2012.

15. Shao, J. Y., S. C. Huang, and Y. H. Pang, "Wilkinson power divider incorporating quasi-elliptic filters for improved out-of-band rejection," *Electron. Lett.*, Vol. 47, No. 23, 1288–1289, Nov. 2011.

16. Zeng, H. Y., G. M. Wang, D. Z. Wei, and Y. W. Wang, "Planar diplexer using composite right-/left-handed transmission line under balanced condition," *Electron. Lett.*, Vol. 48, No. 2, 104–106, Jan. 2012.

17. Zhang, R., L. Zhu, and S. Luo, "Dual-mode dual-band bandpass filter using a single slotted circular patch resonator," *Microwav. Wireless Comp. Lett.*, Vol. 22, No. 5, 233–235, May 2012.

18. Serrano, A. L. C. and F. S. Correra, "A triple-mode bandpass filter using a modified circular patch resonator," *Microw. and Opt. Tech. Lett.*, Vol. 51, No. 1, 178–182, Jan. 2009.